Online ISSN: 2981-0396 Print ISSN: 2981-0388

International Journal of Iron & Steel Society of Iran

Journal Homepage: https://journal.issiran.com/

Research Article

Dry Sliding Wear Resistance of Spheroidal Graphite Cast Iron: The Role of Matrix Microstructure

S. Yans [1], M. N. Yoozbashi *[2], S. Yazdani [3]

[1, 3] Advanced Materials Research Institute, Faculty of Materials Engineering, Sahand University of Technology, Tabriz, Iran
[2] University of Applied Science and Technology, Tabriz, Iran

ARTICLE INFO

Keywords:

Ductile Iron, Matrix Microstructure, Austempering, Pin-on-Disk Test, Dry Sliding Wear, Wear Mechanism.

Article history:

Received 21 April 2025
Received in revised form 23 June 2025
Accepted 16 July 2025

ABSTRACT

Ductile cast irons exhibit excellent wear resistance in frictional applications, primarily due to the inherent lubricating effect of their graphite content. In addition to graphite morphology, the matrix microstructure plays a critical role in governing wear behavior. This study evaluates the influence of various matrix structures on the dry sliding wear performance of spheroidal graphite cast iron. The specimens were produced using the in-mold spheroidizing method and cast into sand molds. To obtain different matrix types, the samples underwent a series of heat treatments, including normalizing, quenching, and austempering at 275 °C, 325 °C, and 375 °C. Microstructural characterization was carried out using optical microscopy and image analysis software. Brinell hardness testing was employed to assess mechanical properties. Dry sliding wear resistance was evaluated using a pin-on-disk tribometer, and the coefficient of friction was monitored throughout the tests. Worn surfaces and associated wear mechanisms were analyzed via scanning electron microscopy (SEM). The results indicated that the quenched sample exhibited the highest wear resistance, with a specific wear rate of 1.9×10^{-6} mm³/N.m. The normalized and austempered samples (at descending order of 275 °C, 325 °C, and 375 °C), followed by the as-cast condition, showed progressively lower performance. The dominant wear mechanism in the quenched sample was identified as a combination of oxidative wear and adhesive wear.

1. Introduction

Ductile iron is a group of iron alloys extensively used in various industrial applications [1-3]. It primarily consists of iron, carbon, and silicon, with additional alloying elements added to enhance mechanical properties, machinability, and castability [4]. Among the key constituents of cast iron is graphite, whose morphology and distribution determine the type of cast iron produced, including gray, white, and ductile variants [5, 6]. In ductile iron, graphite appears in nodular form, which imparts enhanced mechanical properties such as superior strength and ductility [7]. This nodular structure minimizes stress concentration and cleavage effects in the matrix, setting ductile iron apart from other cast iron types [8]. As a result, ductile iron has evolved into

* *Corresponding Author*
Email: n.yoozbashi@uast.ac.ir
Address: University of Applied Science and Technology, Tabriz, Iran
1. M. S., 2. Assistant Professor, 3. Professor

DOI: http://10.22034/IJISSI.2025.2058483.1321
Published by ISSI (Iron & Steel Society of Iran)

a widely adopted engineering material. For instance, it offers higher impact resistance than gray iron, making it suitable for applications involving dynamic or shock loads [9, 10]. It also exhibits significantly lower erosion rates across all impact angles compared to gray iron [11], and its modulus of elasticity is markedly higher at similar graphite contents [12]. These attributes, combined with its excellent wear and corrosion resistance, contribute to its durability. The alloy's ease of casting, good machinability, and well-balanced combination of strength, toughness, and fatigue resistance have enabled it to replace wrought or forged steel components in numerous applications [13-16]. However, under harsh service conditions, such as marine or mining environments, its performance may be limited by wear [8, 17]. Failures due to fracture, corrosion, and wear are among the most frequent in mechanical components and represent a major source of economic loss. Hence, improving wear resistance has become a significant priority for manufacturers [18, 19]. To address this issue, several strategies have been explored, notably heat treatments and surface engineering methods [20-31]. Among these, austempering has emerged as the most widely used technique [32-43]. It results in a matrix composed of ferrite and carbon-enriched retained austenite—collectively termed austempered ductile iron (ADI). ADI's distinctive microstructure enables transformation-induced hardening under applied stress, forming a localized martensitic surface that dramatically enhances wear resistance. Studies have shown that this improvement is attributed to both the lubricating effect of graphite nodules and the strain-induced transformation of retained austenite [44]. Straffellini et al. [45] demonstrated that ADI exhibits a lower coefficient of friction than nitrided steel in dry sliding conditions, primarily due to the graphite phase acting as a solid lubricant. Lu et al. [46] further showed that in Cu–Mo alloyed ADI, carbon-rich austenite transforms into martensite during plastic deformation, contributing to superior wear performance. These observations have been confirmed by other researchers investigating ADI's tribological behavior under various conditions [47-53]. Additionally, other approaches such as local surface reinforcement with Cr-rich inserts [8], quenching and partitioning (Q&P) heat treatment [17], and the incorporation of hard particles in coatings [54] have also been investigated to improve wear resistance. Alloying elements like manganese, nickel, molybdenum, and vanadium have been found to enhance mechanical performance, while cryogenic treatments combined with tempering have shown potential in refining the matrix and boosting both hardness and wear behavior [55, 56]. Graphite morphology, volume fraction, and distribution alongside matrix structure—are fundamental in determining the mechanical and tribological behavior of ductile iron [57]. With graphite comprising about 10–15% of the volume, the matrix microstructure significantly influences the overall material properties [58]. Tailoring this matrix is achievable by manipulating alloy composition, cooling rate during solidification, and post-solidification treatments. According to Lu et al. [59], martensitic and carbide-dispersed martensitic ductile irons offer the highest wear resistance, followed by bainitic, while pearlitic grades exhibit the lowest. Likewise, Zhang et al. [60] found that ductile iron with approximately 78% pearlite provided an optimal balance of wear resistance and mechanical strength.

Given the importance of matrix design in controlling wear behavior, this study investigates the effect of different post-solidification heat treatments—normalizing, quenching, and austempering at multiple temperatures—on the microstructure and wear resistance of spheroidal graphite cast iron. Characterization was performed using optical microscopy (OM), scanning electron microscopy (SEM), image analysis, and hardness and wear testing.

2. Materials and Methods

The ductile iron used in this study had the following chemical composition: Fe-3.5C-2.08Si-0.214Mn-0.017P-0.021S-0.061Mg (wt.%). Samples for evaluating the microstructure and mechanical properties were taken from the lower portion of the Y-block (Fig. 1). The dimensions of the pin and abrasive disk for the wear test were selected to match the specifications in the ASTM G99 standard [61]. Fig. 2. illustrates the wear test setup, including the geometries of the pin and disk. The pin specimens were cylindrical, with one face designated for contact with the abrasive surface. The disk was made of 100Cr6 steel, hardened to 65 HRC, and featured a surface roughness of 0.6 μm.

A lathe machine was used to prepare the specimens, with a machining allowance of approximately 0.2 mm. To ensure uniformity after heat treatment and facilitate testing, the wear test pins and microstructural specimens were temporarily fabricated as a single combined unit (Fig. 3). After heat treatment, the microstructural specimens were separated from the pin using wire cutting and were then subjected to relevant evaluations.

To produce different microstructures, including pearlitic, martensitic, and ausferritic types, the samples were subjected to five heat treatment conditions: normalizing, quenching, and austempering at 275 °C, 325 °C, and 375 °C. Details of the heat treatment procedures are listed in Table 1.

Microstructural analysis was conducted using an Olympus PMG3™ optical microscope with up to 1000×magnification. Images were taken at various magnifications for both as-cast and heat-treated samples. Brinell hardness testing was performed using ESEWAY™ equipment, and hardness values were reported as average values with 95% confidence intervals.

Wear tests were performed using a pin-on-disk device (AMI POD 1 model) following the ASTM G99 standard. Test parameters included a normal force of 50 N, a sliding speed of 0.05 m/s, and a total sliding distance of 500 meters. To ensure accuracy in weight-loss measurement, the pin and disk surfaces were ultrasonically cleaned in acetone and 99.98% ethyl alcohol, each for 14 minutes, in a clean container. Each pin was weighed three times before and after the test using a precision balance with an accuracy of 0.0001 mg. Wear resistance was assessed based on the weight loss and its associated uncertainty at a 95% confidence level.

Surface morphology and wear mechanisms were examined using a LEO 440i scanning electron microscope (SEM). Prior to imaging, the worn surfaces were gold-coated using a sputtering system under an argon plasma environment.

3. Results and Discussion

3.1. Microstructure

As-cast condition: Fig. 4. illustrates the microstructure of ductile iron in the as-cast condition. The distribution and morphology of phases in cast iron are strongly influenced by carbon and silicon content. As the equivalent carbon content increases and approaches the eutectic point, the matrix becomes predominantly ferritic, reaching up to 78%. Consequently, a coarse-grained matrix is formed, containing a small amount of approximately 9% pearlite. Additionally, increasing the silicon content to 2% by weight enhances graphitization in cast iron. Table 2. presents the volume percentages of the phases in the microstructure of cast iron, which were determined using ImageJ analysis software.

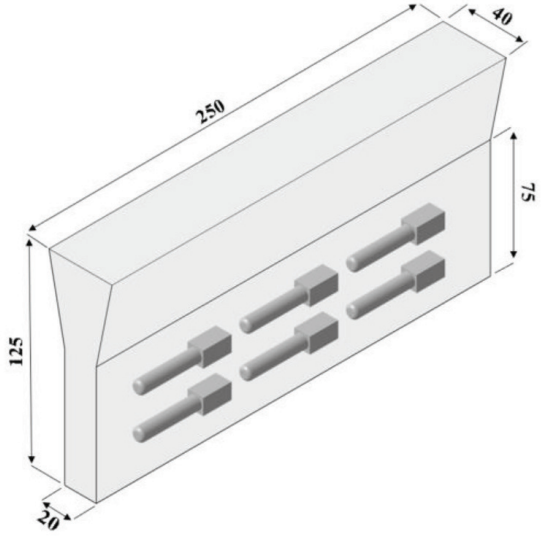

Fig. 1. Schematic illustration of the Y-block showing the sampling locations used for microstructural analysis, hardness testing, and dry sliding wear experiments. The dimensions of the Y-block are also provided (in mm).

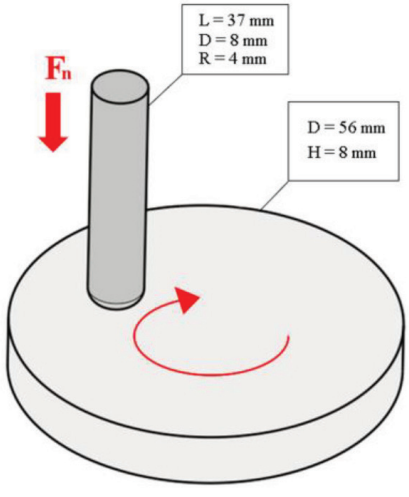

Fig. 2. Schematic of the experimental setup for the wear test, indicating the dimensions of the pin and the abrasive disk.

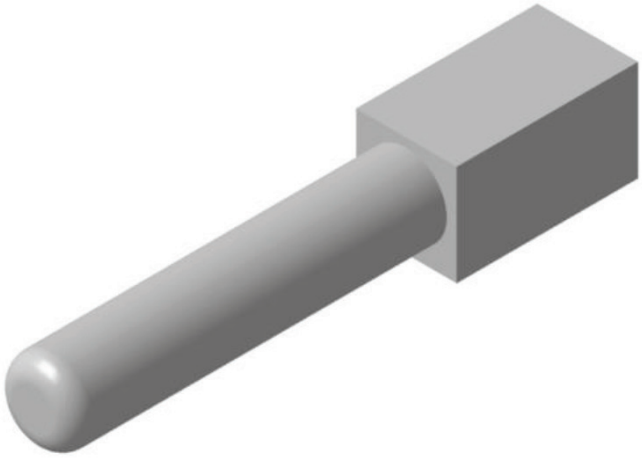

Fig. 3. Schematic illustration of the integrally machined test specimen, consisting of a cylindrical wear pin and an attached cubic section for microstructural evaluation.

Table 1. Heat treatment parameters for producing different microstructures.

Identification	Heat treatment	Austenitizing	Subsequent treatment
Normalized	Air Cooling	900 °C, 60 min	Cooling in air
Quenched	Brine Quenching	900 °C, 60 min	Quenching in brine
Aus375	Austempering at 375 °C	900 °C, 120 min	Quenching in salt bath + Austempering at 375 °C (60 min) + Air cooling
Aus325	Austempering at 325 °C	900 °C, 120 min	Quenching in salt bath + Austempering at 325 °C (60 min) + Air cooling
Aus275	Austempering at 275 °C	900 °C, 120 min	Quenching in salt bath + Austempering at 275 °C (60 min) + Air cooling

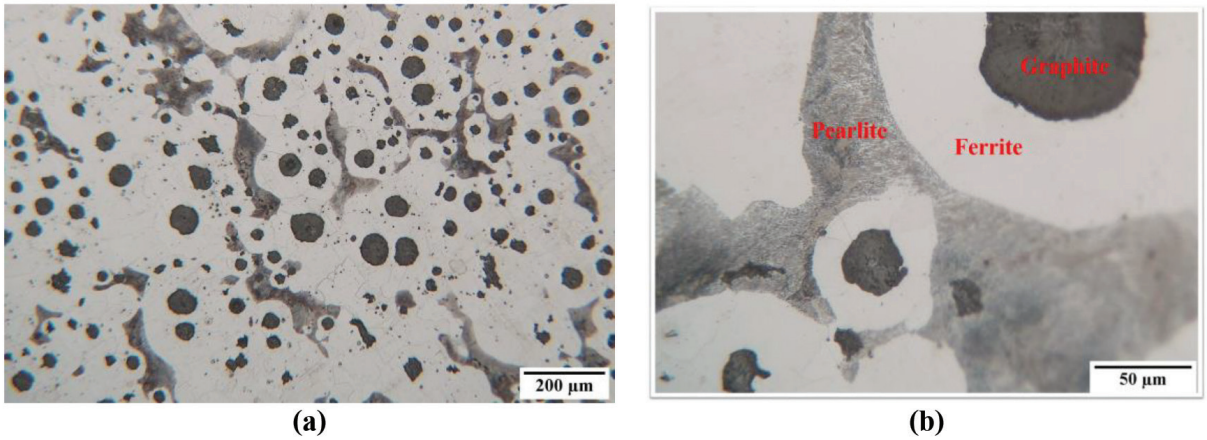

(a) **(b)**

Fig. 4. Optical microscopy images of ductile cast iron in the as-cast condition, revealing a ferrite-dominated microstructure with graphite nodules and pearlite islands, shown at two different magnifications (a and b).

Table 2. Microstructural characteristics and phase volume fractions of ductile iron in the as-cast condition.

Volume Fraction of Phases (Vol. %)	Nodularity	Nodules count (No./mm^2)
78% Ferrite + 9% Pearlite + 13% Graphite	> 90	300

Normalized condition: Normalization is carried out to produce a uniform microstructure of fine pearlite. This heat treatment relies on nucleation and growth mechanisms, occurring through a diffusion-controlled phase transformation where austenite converts into ferrite and cementite. During cooling, the accelerated formation rate of ferrite and pearlite causes: 1) Reduced grain size in ferrite/cementite structures and 2) Decreased interlamellar spacing in pearlite colonies. These microstructural refinements lead to the characteristic appearance of fine, well-distributed pearlite within the cast iron's matrix. The impact of elements in the chemical composition on the fineness of pearlite in the microstructure can be attributed to silicon and manganese, two key elements in the chemical composition of cast iron. Generally, in cast iron, silicon and manganese play a significant role in forming fine pearlite. Fine pearlite can be achieved if the cast iron contains less than 2% silicon by weight and has a manganese content between 0.3% and 0.5% by weight.

Fig. 5. displays microstructure images of ductile iron, which consists of 93% pearlite and 7% ferrite, following normalization. Generally, in the microstructure of cast irons, a higher pearlite nucleation potential corresponds to a lower ferrite volume fraction. According to the mentioned theory, the cast iron under investigation contains 2 wt.% silicon and 0.214 wt.% manganese. This composition significantly enhances the nucleation and refinement of pearlite compared to its as-cast state.

Quenched condition: Rapid quenching in brine produces a fine martensitic structure with retained austenite; the resulting hardness from quenching depends on the carbon content of the martensite and the volume fraction of martensite in the matrix. Fig. 6. illustrates the microstructure of cast iron following quenching in brine. Brine quenching provides a higher cooling rate compared to oil or air, resulting in finer martensite. The salt in the brine prevents air bubbles from forming on the samples, allowing a larger cross-sectional area to be covered by the solution.

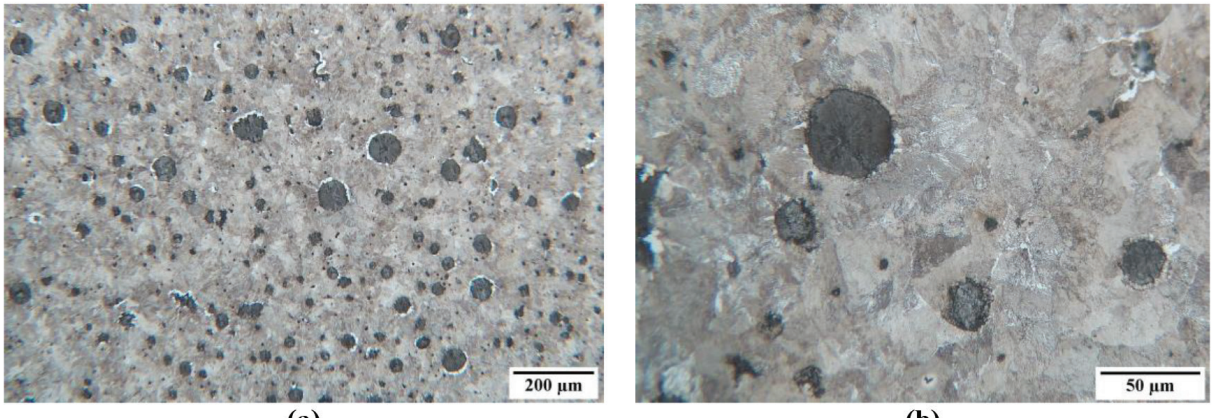

Fig. 5. Optical micrographs of ductile iron after normalization, showing a pearlite-dominated microstructure at two different magnifications (a and b).

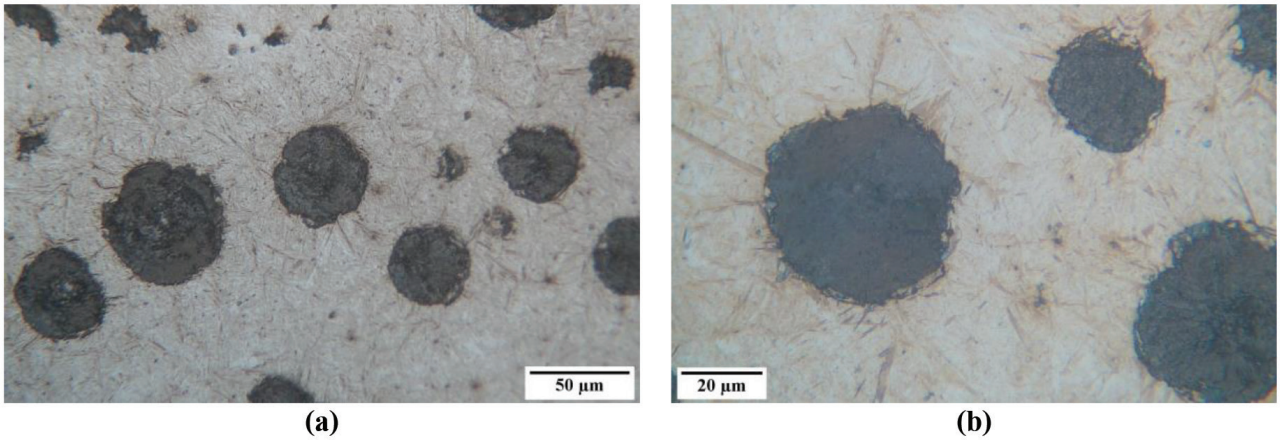

Fig. 6. Optical micrographs of ductile iron after brine quenching, revealing a martensite-dominated microstructure at two different magnifications (a and b).

Austempered condition: The main goal of austempering heat treatment in ductile cast iron is to develop an ausferritic microstructure consisting of bainitic ferrite and carbon-enriched retained austenite, which imparts enhanced mechanical properties. Similar microstructures have been reported in bainitic steels subjected to isothermal transformation, known for their superior strength–toughness balance [62-66]. Fig. 7. presents micrographs of cast iron samples subjected to austempering at different temperatures. In these images, the dark lath-shaped regions represent bainitic ferrite, while the lighter films between them, although not always clearly visible, correspond to thin layers of retained austenite. Additionally, coarse white zones indicate the presence of blocky austenite that did not fully transform during heat treatment. The morphology of the ausferritic structure is highly temperature-dependent, as austempering is governed by nucleation and diffusion-controlled growth. At lower austempering temperatures, reduced carbon mobility leads to finer ferrite plates and slower formation of retained austenite. This results in a more refined ausferritic structure with a lower volume fraction of austenite.

In contrast, higher austempering temperatures promote increased carbon diffusion, leading to the formation of coarser austenite and a reduction in the volume of ferrite. According to the incomplete transformation theory, blocky austenite tends to form between the bainitic ferrite laths under these conditions. With increasing temperature, both the quantity and size of blocky austenite regions tend to rise, while the ferrite fraction decreases in accordance with the lever rule. Due to the high silicon content and the abundance of graphite nodules in the studied alloy, ferrite nucleation is promoted. This accelerates the bainitic transformation and restricts the formation of blocky retained austenite [67]. As a result, the final microstructure becomes more uniform and less prone to the negative mechanical effects typically associated with blocky austenite.

3.2. Mechanical properties

Hardness variations: Fig. 8. displays the Brinell hardness number (BHN) variations for the studied cast iron in both as-cast and heat-treated conditions. It is evident that the hardness of the cast iron in the normalized state has increased by approximately 50% compared to the as-cast state. The formation of fine-grained cast iron and the creation of a fine pearlite matrix due to air cooling have resulted in the cast iron having a higher hardness than in the as-cast state. Among the austempered samples, the 275°C condition exhibited the highest hardness, second only to the quenched sample. The lower ausferritic structure, comprising fine layers of ferrite and retained austenite, resulted in higher hardness in the cast iron.

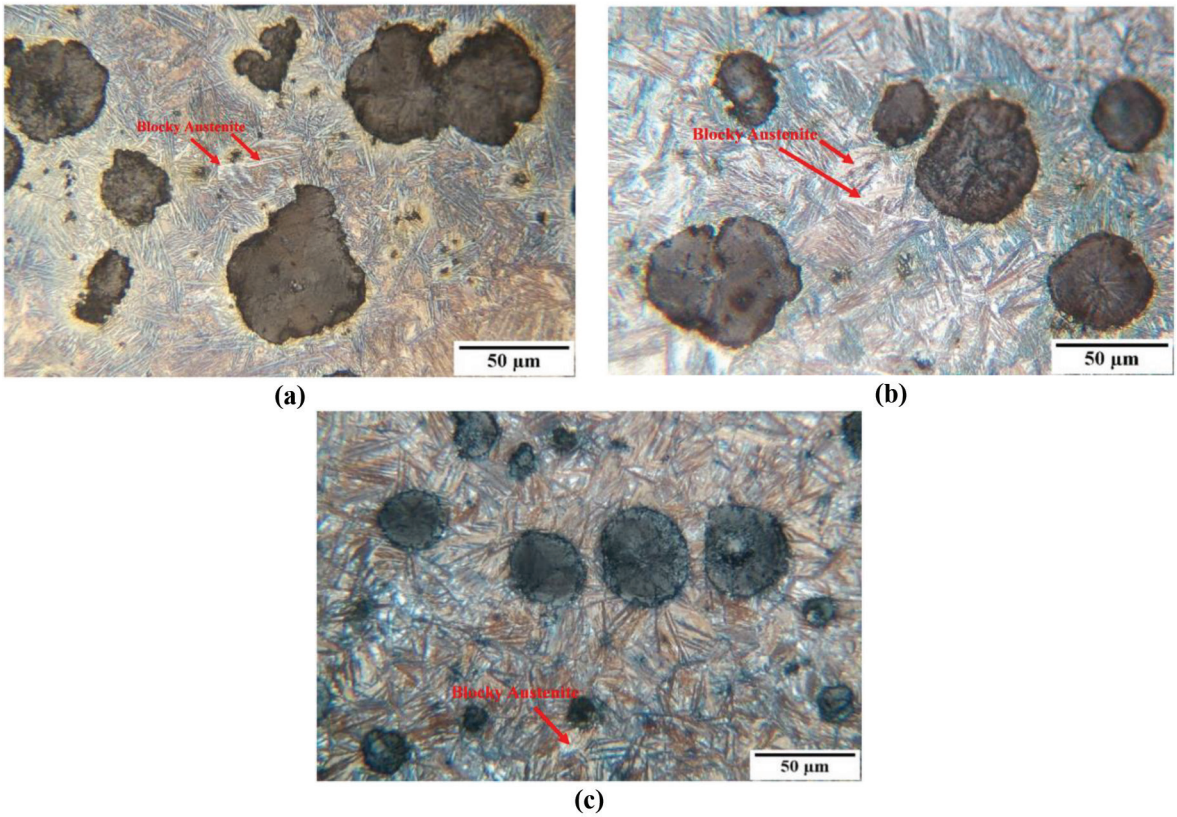

Fig. 7. Optical micrographs of ductile iron austempered at 275 °C (a), 325 °C (b), and 375 °C (c), illustrating the temperature-dependent evolution of the ausferritic microstructure and the presence of blocky austenite.

Increasing the austempering temperature to 325°C and forming a high ausferritic structure results in a decrease in the hardness of cast iron. This decrease is attributed to the coarsening of the ferrite layers and an increase in the volume fraction of retained austenite. Subsequently, austempering at 375°C further coarsens the ausferritic structure, continuing the trend of decreasing hardness compared to austempering at 325°C. However, the reduction in hardness is less pronounced at 375°C than it is at 325°C.

Wear resistance: In this section, the quantitative results of the wear test, including the weight loss and wear rate of samples, are examined. Factors such as the microstructure of the matrix, hardness, and the number of graphite nodules play a significant role in the wear behavior of cast irons. In some cases, the high hardness of the microstructure due to the matrix has not contributed to wear resistance, while a high volume fraction of graphite has resulted in high wear resistance.

Figs. 9 and 10. illustrate the weight loss and specific wear rate of cast iron in its as-cast and heat-treated states, respectively. In this section, the analysis of the discussions is based exclusively on the weight loss of the samples and the wear rate.

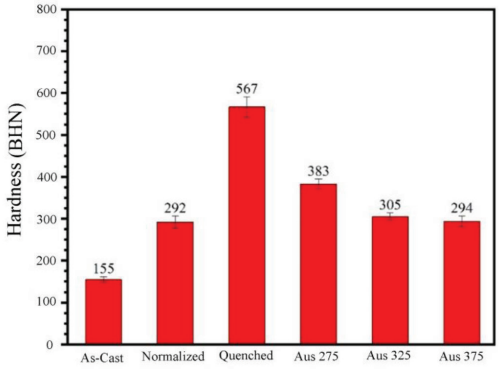

Fig. 8. Brinell hardness values (BHN) of ductile iron in the as-cast condition and after various heat treatments, including normalization, quenching, and austempering at 275 °C, 325 °C, and 375 °C.

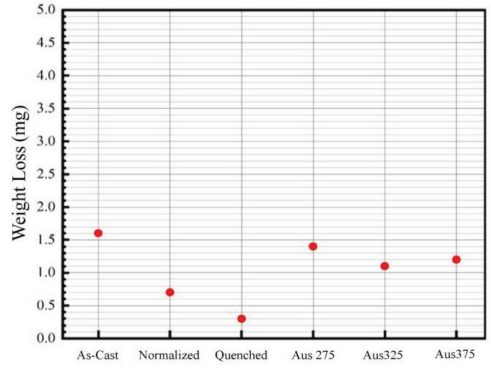

Fig. 9. Measured weight loss of ductile iron samples during dry sliding wear tests in the as-cast state and after different heat treatments, including normalization, quenching, and austempering at 275 °C, 325 °C, and 375 °C.

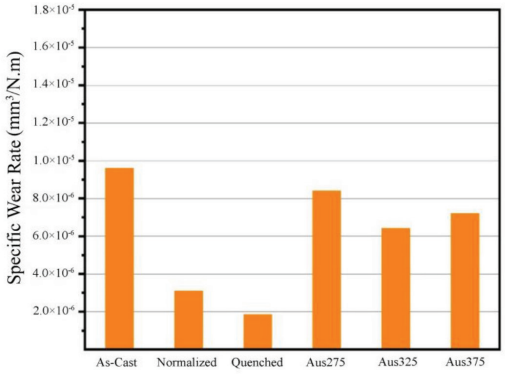

Fig. 10. Specific wear rate of ductile iron samples under dry sliding conditions, comparing the as-cast state with heat-treated conditions including normalization, quenching, and austempering at 275 °C, 325 °C, and 375 °C.

Spheroidal graphite in the microstructure of ductile iron functions as a lubricating phase in the wear track [68], reducing the coefficient of friction and thereby preventing further weight loss. Consequently, the presence of graphite enhances the wear resistance of ductile irons in the as-cast state.

The fine pearlite microstructure found in both cast irons and steels demonstrates exceptional dry sliding wear resistance. This stems from pearlite's layered structure of alternating cementite and ferrite phases, where reduced interlamellar spacing (the distance between these layers) directly correlates with enhanced wear resistance [69, 70]. Microstructural studies clearly show that the volume fraction of pearlite in cast iron increases with normalizing treatment. Consequently, the presence of graphite with a high nodule count in a matrix of fine pearlite results in a further enhancement of wear resistance in the normalized condition.

Cast iron in the quenched state exhibits the highest wear resistance among all samples with different microstructures. X-ray diffraction analysis, conducted to study this sample more closely, reveals that the volume fraction of martensite in the cast iron is approximately 98%. The significant presence of fine martensite, combined with a high volume fraction of spherical graphite that act as a lubricant, results in excellent wear resistance and achieves the lowest wear rate. Additionally, this cast iron did not produce any noise during wear and friction at the start of the test or throughout the testing process.

A comparison of the wear behavior of austempered samples at different temperatures shows that the wear resistance of cast irons changes only slightly with increasing austempering temperature. Additionally, austempered samples exhibit lower wear resistance compared to quenched and normalized samples. This is likely due to the coexistence of soft graphite phase and a relatively soft ausferrite microstructure in austempered samples. Typically, in the wear behavior of cast irons, the theory holds that a hard matrix provides high wear resistance [71]. However, some studies have shown the opposite. Perhaps the theory can be refined by suggesting that optimal wear resistance is achieved when a soft phase, such as graphite, is combined with a hard matrix, like martensite or fine pearlite, or when a hard phase, such as carbide, is adjacent to a soft matrix, like ausferrite.

Wear mechanisms: In this section, diagrams of friction coefficients, microscopic images of wear surfaces, and wear mechanisms of sample with high wear resistance (sample in a quenched condition) are discussed.

The presence of solid or liquid lubricants, or an oxide film formed in the wear path, can reduce the coefficient of friction. Surface roughness, the tension generated between the two surfaces during wear, or debris in the wear path can increase the coefficient of friction, typically indicating a decrease in wear resistance. Coefficient of friction diagrams typically consist of two stages: running-in and stable, which often exhibit slight fluctuations at the beginning of the wear path. If the contact surface becomes smooth during the running-in stage, a stable coefficient of friction may be maintained. However, if the quality of the surfaces is affected by factors that alter roughness or create tension in the wear path, the fluctuations in the diagram will likely increase or decrease, resulting in no stable and constant coefficient of friction [72].

Fig. 11. shows the friction coefficient graph of cast iron in the quenched condition. According to the figure, from the beginning of wear to a distance of 30 meters, the friction coefficient increases, likely due to the initial roughness of the pin surface resulting from the quenching heat treatment. Then, following a peak, the friction coefficient decreases, and this downward trend continues until the test concludes with the lowest friction coefficient. The fluctuations in the friction coefficient are narrower and more uniform, indicating the high abrasion resistance of this sample. The initial drop in the friction coefficient at early distances, followed by reaching a stable state and maintaining this trend, suggests the lubricating effect of graphite in the quenched sample. This has contributed to high abrasion resistance and the lowest abrasion rate.

Fig. 12. shows the wear surface of the quenched sample at two different magnifications. The surface exhibits minimal damage, characterized by shallow wear grooves and a relatively smooth topography with fewer surface irregularities. Within the wear track, the scratches appear well-aligned in the direction of sliding, indicating a high surface hardness that is consistent with the presence of a martensitic matrix. Graphite nodules in the matrix have contributed to lubrication during sliding, reducing friction and material removal. However, they have also acted as potential sites for crack initiation, particularly where voids or debonding occur around the graphite particles. This is evident in Fig. 12(b). where a crack is observed developing from a region once occupied by graphite. Such cracks tend to grow through the coalescence of microcracks initiated at stress concentrators. Additionally, small oxide-like particles are visible in the wear path, suggesting localized oxidation during sliding. Considering both the lubricating effect of graphite and the presence of adhesive oxide particles, the dominant wear mechanism in the quenched sample can be identified as a combination of oxidative wear and adhesive wear.

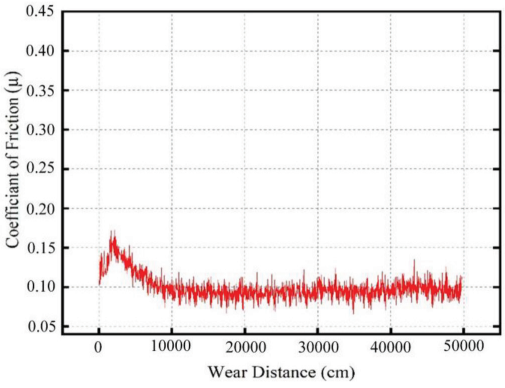

Fig. 11. Variation of the coefficient of friction (μ) with sliding distance for ductile iron in the quenched condition under dry sliding wear.

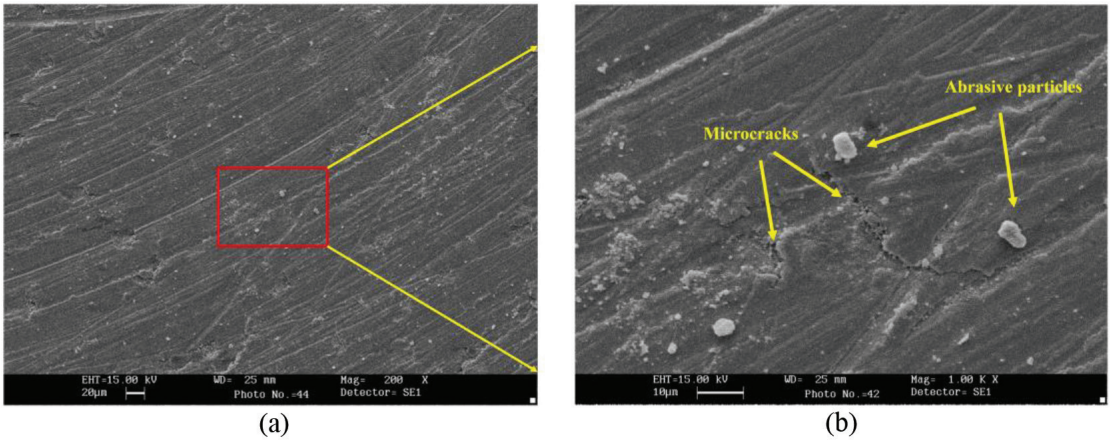

Fig. 12. SEM images of the worn surface of the quenched ductile iron sample: (a) low-magnification view showing aligned wear tracks, and (b) high-magnification view highlighting microcracks and embedded abrasive particles.

4. Conclusions

This study investigated the influence of different matrix microstructures, including fine pearlite, ausferrite, and martensite, on the wear behavior of ductile iron under dry sliding conditions. The main findings can be summarized as follows:

- A high-volume fraction of graphite, present both in the as-cast and heat-treated conditions, effectively acts as a solid lubricant during sliding, thereby enhancing wear resistance.
- Among all tested conditions, the highest hardness value of 567 BHN was recorded in the quenched sample, while the as-cast sample showed the lowest hardness of approximately 155 BHN.
- The best wear performance was observed in samples with a hard matrix combined with uniformly distributed graphite nodules. In particular, the quenched and normalized samples exhibited superior wear resistance compared to other heat treatment conditions.
- The quenched ductile iron demonstrated the highest wear resistance, with a specific wear rate of 1.9×10^{-6} mm³/N.m. In contrast, the as-cast sample exhibited the lowest resistance, with a specific wear rate of 9.5×10^{-6} mm³/N.m.
- The evolution of the friction coefficient in the quenched samples, showing a stable and decreasing trend during sliding, further confirms their excellent wear resistance and surface integrity.
- The primary wear mechanisms identified in the quenched samples were oxidative wear and adhesive wear, as evidenced by SEM observations and the presence of oxide particles along the wear track.

References

[1] Labrecque C, Gagne M, Ductile iron: Fifty years of continuous development, Can Metall Q. 1998; 37(5): 343–78.

[2] Tiedje N.S, Solidification, processing and properties of ductile cast iron, Mater Sci Technol. 2010; 26(5): 505–14.

[3] Bustillo Revuelta M, Bustillo Revuelta M, Metals and Alloys, In: Construction Materials: Geology, Production and Applications. 2021: 435–75.
[4] Chikali P, Shinde V, Analysis of machinability in ductile iron casting, Mater Today Proc. 2020; 27: 584–8.
[5] Olawale J, Ibitoye S, Oluwasegun K, Processing techniques and productions of ductile iron: A review, Int J Sci Eng Res. 2016; 7(9): 397–423.
[6] Karimi M, Structure of Cast Iron and Its Application in Industry, J Eng Ind Res. 2023; 4(2): 77–85.
[7] Jenkins L.R, Forrest R, Ductile Iron. In: Properties and Selection: Irons, Steels, and High-Performance Alloys, ASM International. 1990: 33–55.
[8] Podgornik B, Vizintin J, Thorbjornsson I, et al. Improvement of ductile iron wear resistance through local surface reinforcement, Wear. 2012; 274: 267–73.
[9] Cherkashin S, Installation of the Pipelines Made of Ductile Iron (DI) with the Usage of Horizontal-directional Drilling Technique (HDD) for Water Supply Treatment Service and Sewerage Pipelines Construction and Reconstruction, Procedia Eng. 2016.
[10] Zhang Y, Guo E, Wang L, et al. Research and Analysis of the Effect of Heat Treatment on Damping Properties of Ductile Iron, Open Phys.
[11] Yıldızlı K, Karamış M, Nair F, Erosion mechanisms of nodular and gray cast irons at different impact angles, Wear. 2006; 261(5–6): 622–33.
[12] Speich G, Schwoeble A, Kapadia B, Elastic moduli of gray and nodular cast iron, J Appl Mech. 1980; 47: 821–6.
[13] Imasogie B. Ductile Iron Production Technology: A Review. Ife J Technol. 2015; 23(2): 24–35.
[14] Sahoo S.K, A study on the effect of austempering temperature, time and copper addition on the mechanical properties of austempered ductile iron [dissertation]. 2012.
[15] Akinribide O.J, Ogundare O.D, Oluwafemi O.M, et al. A review on heat treatment of cast iron: phase evolution and mechanical characterization. Materials. 2022; 15(20): 7109.
[16] Chanda M, Chanda M, Metals and Alloys, In: Science of Engineering Materials: Materials. 1979: 02–35.
[17] Wang Z, Huang B, Chen H, et al. The effect of quenching and partitioning heat treatment on the wear resistance of ductile cast iron, J Mater Eng Perform. 2020; 29:4 370–8.
[18] Penghui Y, Hanguang F, Guolu L, et al. Microstructures and properties of carbidic austempered ductile iron containing Fe_3C particles and superfine ausferrite. Mater Des. 2020; 186: 108363.
[19] Zhang H, Wu Y, Li Q, et al. Mechanical properties and rolling-sliding wear performance of dual phase austempered ductile iron as potential metro wheel material. Wear. 2018; 406: 156–65.
[20] Sckudlarek W, Krmasha M.N, Al-Rubaie K.S, et al. Effect of austempering temperature on microstructure and mechanical properties of ductile cast iron modified by niobium, J Mater Res Technol. 2021; 12: 2414–25.
[21] Hsu C.H, Chen H.W, Lin C.Y, et al. Improvement in surface hardness and wear resistance of ADI via arc-deposited CrAlSiN multilayer films, Materials. 2025; 18(9).
[22] Záhon L, Kuchař J, Horník J, et al. Laser surface hardening of austempered ductile iron (ADI), Coatings. 2024; 14(8).
[23] Wang X, Du Y, Liu C, et al. Tribological behaviour and wear mechanism of ADI with different hardness values, Mater Sci Technol. 2023; 39(16): 2409–16.
[24] Liu C, Du Y, Wang X, et al. Comparison of the tribological behavior of quench-tempered ductile iron and austempered ductile iron with similar hardness, Wear. 2023; 520–521: 204668.
[25] Hu Z, Du Y, Mechanical and tribological behavior of austempered ductile iron (ADI) under dry sliding conditions, Lubricants. 2023; 11(4).
[26] Hsu C.H, Lin C.Y, You W.S, Microstructure and dry/wet tribological behaviors of 1% Cu-alloyed austempered ductile iron, Materials. 2023; 16(6).
[27] Zhiwang S, Xiaohui Z, Yufan S, et al. Microstructure and properties of high manganese carbidic austempered ductile iron, Trans Indian Inst Met. 2022; 75(3): 833–42.
[28] Yunlong L, Rong N, Yufan S, et al. Carbidic austempered ductile iron: current status and future prospects, J Mater Eng Perform. 2022; 31(5): 3409–17.
[29] Khidasheli N, Gordeziani G, Gvazava S, et al. Influence of structural parameters on the wear resistance of ADI during dry sliding friction, In: Lecture Notes in Networks and Systems. 2022.
[30] Colombo D.A, Quintana J.P, Mandri A.D, et al. Sliding wear performance of TiAl-based nitride coatings deposited on ADI by cathodic arc deposition and plasma based ion implantation and deposition, Tribol Mater Surf Interfaces. 2022; 16(4): 303–16.
[31] Benam A.S, Yazdani S, Avishan B, Effect of shot peening process on fatigue behavior of an alloyed austempered ductile iron, China Foundry. 2011; 8(3): 325–30.
[32] Penghui Y, Hanguang F, Xiangwei Z, et al. Wear behavior of CADI obtained at different austenitizing temperatures, Tribol Int. 2019; 140: 105876.
[33] Yazdani S, Bayati H, Elliott R, The influence of cobalt on the austempering reaction in ductile cast iron, Int J Cast Met Res. 2001; 13(6): 317–26.
[34] Yazdani S, Elliott R, Influence of molybdenum on austempering behaviour of ductile iron - Part 3, Mater Sci Technol. 1999; 15(8): 885–95.
[35] Yazdani S, Elliott R, Influence of molybdenum on austempering behaviour of ductile iron - Part 4, Mater Sci Technol. 1999; 15(8): 896–902.
[36] Yazdani S, Elliott R, Influence of molybdenum on austempering behaviour of ductile iron - Part 1, Mater

Sci Technol. 1999; 15(5): 531–40.
[37] Yazdani S, Elliott R, Influence of molybdenum on austempering behaviour of ductile iron - Part 2, Mater Sci Technol. 1999; 15(5): 541–6.
[38] Li P, Du Y, Zhang M, et al. Effects of carbon content in parent austenite on tribological behavior of austempered ductile iron, J Mater Eng Perform. 2025.
[39] Wieczorek A.N, Ni-Cu alloyed austempered ductile iron resistance to multifactorial wear, Lubricants. 2024; 12(4).
[40] Myszka D, Wieczorek A.N, Skołek E, et al. Abrasive wear resistance of ultrafine ausferritic ductile iron intended for the manufacture of gears for mining machinery, Materials. 2023; 16(12).
[41] Wieczorek A.N, Wójcicki M, Drwięga A, et al. Abrasive wear of mining chain drums made of austempered ductile iron in different operating modes, Materials. 2022;15(8).
[42] Gecu R, Microstructure, mechanical, and wear properties of Al-alloyed austempered ductile irons, Tribol Trans. 2022; 65(5): 952–62.
[43] Galagali R.M, Ashok M.H, Khadakbhavi V.M, et al. Effect of speed and temperature on the tribological behaviour of ADI, In: Lecture Notes in Intelligent Transportation and Infrastructure, Springer. 2022: 329–37.
[44] Mussa A, Krakhmalev P, Bergström J, Wear mechanisms and wear resistance of austempered ductile iron in reciprocal sliding contact, Wear. 2022; 498: 204305.
[45] Straffelini G, Pellizzari M, Maines L, Effect of sliding speed and contact pressure on the oxidative wear of austempered ductile iron. Wear. 2011; 270(9–10): 714–9.
[46] Lu G.X, Zhang H, Sliding wear characteristics of austempered ductile iron with and without laser hardening, Wear. 1990; 138(1–2): 1–12.
[47] Sellamuthu P, Samuel D.H, Dinakaran D, et al. Austempered ductile iron (ADI): influence of austempering temperature on microstructure, mechanical and wear properties and energy consumption, Metals. 2018; 8(1): 53.
[48] Zammit A, Abela S, Wagner L, et al. Tribological behaviour of shot peened Cu–Ni austempered ductile iron, Wear. 2013; 302(1–2): 829–36.
[49] Wen F, Zhao J, Zheng D, et al. The role of bainite in wear and friction behavior of austempered ductile iron, Materials. 2019; 12(5): 767.
[50] Chiniforush E.A, Yazdani S, Nadiran V, The influence of chill thickness and austempering temperature on dry sliding wear behaviour of a Cu-Ni carbidic austempered ductile iron (CADI), Kovove Mater. 2018; 56(4): 213–21.
[51] Chiniforush E.A, Rahimi M.A, Yazdani S, Dry sliding wear of Ni alloyed austempered ductile iron, China Foundry. 2016; 13(5): 361–7.
[52] Yazdani S, Rahimi M.A, Wear behavior of an austempered ductile iron containing Mo-Ni-Cu. In: PRICM 5. 2005: 199–202.
[53] Yans S, Yoozbashi M.N, Yazdani S, Microstructure and wear resistance in low carbon-equivalent ductile iron with carbide particles, Int J Met Cast. 2025.
[54] Aal A.A, Ibrahim K.M, Hamid Z.A, Enhancement of wear resistance of ductile cast iron by Ni–SiC composite coating, Wear. 2006; 260(9–10): 1070–5.
[55] Boulifa I, Hadji A, Study of the influence of alloying elements on the mechanical characteristics and wear behavior of a ductile cast iron, Frat Ed Integrità Strutt. 2021; 15(56): 74–83.
[56] Šolić S, Godec M, Schauperl Z, et al. Improvement in abrasion wear resistance and microstructural changes with deep cryogenic treatment of austempered ductile cast iron (ADI), Metall Mater Trans A. 2016; 47: 5058–70.
[57] Hafiz M, Mechanical properties of SG-iron with different matrix structure, J Mater Sci. 2001; 36: 1293–300.
[58] Toktaş G, Tayanç M, Toktaş A, Effect of matrix structure on the impact properties of an alloyed ductile iron, Mater Charact. 2006; 57(4–5): 290–9.
[59] Lu Z.L, Zhou Y.X, Rao Q.C, et al. An investigation of the abrasive wear behavior of ductile cast iron, J Mater Process Technol. 2001; 116(2–3): 176–81.
[60] Zhang H, Wu Y.X, Li Q.J, et al. Effect of matrix structure on mechanical properties and dry rolling–sliding wear performance of alloyed ductile iron, J Iron Steel Res Int. 2019; 26: 888–97.
[61] ASTM G99-23. Standard Test Method for Wear and Friction Testing with a Pin-on-Disk or Ball-on-Disk Apparatus. ASTM Int; 2023.
[62] Yoozbashi M, Yazdani S, Wang T, Design of a new nanostructured, high-Si bainitic steel with lower cost production, Mater Des. 2011; 32(6): 3248–53.
[63] Yoozbashi M, Yazdani S. Mechanical properties of nanostructured, low temperature bainitic steel designed using a thermodynamic model. Mater Sci Eng A. 2010;527(13–14):3200–5.
[64] Yoozbashi M.N, Zolfaghari R, Yazdani S, et al. Other aspects of the impact fracture toughness-microstructure relationship in nano-bainitic steels, J Mater Eng Perform. 2024: 1–9.
[65] Avishan B, Yazdani S, Nedjad S.H, Toughness variations in nanostructured bainitic steels, Mater Sci Eng A. 2012; 548: 106–11.
[66] Mousalou H, Yazdani S, Avishan B, et al. Microstructural and mechanical properties of low-carbon ultra-fine bainitic steel produced by multi-step austempering process, Mater Sci Eng A. 2018; 734: 329–37.
[67] Putatunda S.K, Development of austempered ductile cast iron (ADI) with simultaneous high yield strength and fracture toughness by a novel two-step austempering process, Mater Sci Eng A. 2001; 315(1–2): 70–80.

[68] Batra U, Batra N, Sharma J, Wear performance of Cu-alloyed austempered ductile iron, J Mater Eng Perform. 2013; 22: 1136–42.
[69] Elliott R. Cast iron technology. 1988.
[70] Chaves A.P.G, Centeno D.M.A, Masoumi M, et al. Effect of the microstructure on the wear resistance of a pearlitic steel, Mater Res. 2020; 23: e20190605.
[71] Laino S, Ortiz H.R, Dommarco R.C, The influence of austempering temperature on the wear resistance of ductile iron under two different tribosystems. ISIJ Int. 2009;49(1):132–8.
[72] Leiro A, Kankanala A, Vuorinen E, et al. Tribological behaviour of carbide-free bainitic steel under dry rolling/sliding conditions, Wear. 2011; 273(1): 2–8.